[PHOTOLYTIC MASS LOSS OF SECONDARY ORGANIC AEROSOL DERIVED FROM PHOTOOXIDATION OF BIOMASS BURNING FURAN PRECURSORS]

A Dissertation
Presented to
The Academic Faculty
Dr. Pengfei Liu
Dr. Nga Lee (Sally) Ng
Dr. Rodney Weber

by

[Nara Shin]

In Partial Fulfillment
of the Requirements for the Degree
[Master of Science] in the
[School of Earth and Atmospheric Science]

Georgia Institute of Technology
[August 2023]

[PHOTOLYTIC MASS LOSS OF SECONDARY ORGANIC AEROSOL DERIVED FROM PHOTOOXIDATION OF BIOMASS BURNING FURAN PRECURSORS]

Approved by:

Dr. Pengfei Liu, Thesis Advisor
School of Earth and Atmospheric Science
Georgia Institute of Technology

Dr. Nga Lee (Sally) Ng, Thesis Advisor
School of Chemical and Biomolecular Engineering
Georgia Institute of Technology

Dr. Rodney Weber, Committee Member
School of Earth and Atmospheric Science
Georgia Institute of Technology

Date Approved: [July, 28th, 2023]

[To the students of the Georgia Institute of Technology]

ACKNOWLEDGEMENTS

I wish to express my sincere appreciation to the committee members involved in this project. First and foremost, I would like to extend my heartfelt thanks to my advisors, Dr. Pengfei Liu and Dr. Sally Ng who made this work possible. Their expertise, guidance, advice, dedication and support have led me to carry out this project and through all the stages of the Master's program. From the initial stages of conceptualization to the final analysis of my research, their insights and recommendations have been invaluable. Their recommendations are always helpful during my time in the program and the analysis of my research. It was definitely a golden opportunity to do the projects with them. There are times I got lost during the project, but their guidance was above and beyond to put me back on track and I wouldn't be able to make it through without them.

Secondly, I would also like to thank Dr. Rodney Weber who gave me the most valuable lessons throughout the entire program of study. His teachings and mentorship have profoundly impacted my academic and personal growth. Taking his aerosol class was a true privilege, and I have immense respect and admiration for him as a professor.

Furthermore, I would also like to extend my appreciation to all my colleagues in both research labs. Their collaboration and assistance have been crucial throughout this project. Their expertise and willingness to offer guidance whenever I faced challenges were indispensable, and I am grateful for their support. Without them, this journey would not have been possible.

Lastly, I would like to thank my families in both South Korea and here in the United States, as well as my friends for their support and understanding. Their love, encouragement, and belief in my abilities have been the driving force to continue researching. I am truly grateful for their presence in my life.

In conclusion, I extend my deepest appreciation to each and every individual who has contributed to my journey at Georgia Tech. Your guidance, support, and belief in my abilities have been impactful in my life bringing this endeavor to fruition. Thank you all once again for your unwavering support and for being an integral part of this remarkable journey.

TABLE OF CONTENTS

LIST OF TABLES

LIST OF FIGURES

SUMMARY

Direct photolysis as a potentially important chemical loss pathway for atmospheric organic aerosol (OA) is increasingly recognized, but remains highly uncertain, particularly for secondary organic aerosol (SOA) derived from biomass-burning (BB) precursors. Here we present the measurements of photolytic mass change of SOA derived from the photooxidation of three furan precursors, 3-methylfuran, 2-methylfuran, and furfural in an environmental chamber for both dry and humid conditions. The SOA was collected on crystal sensors, and the mass losses by photolysis under 300 nm and 340 nm UV were continuously monitored using a highly sensitive quartz-crystal microbalance (QCM). By incorporating measurements and modeling, our results suggest that SOA from furan species can lose 10-40% mass by direct photolysis under solar radiation over their typical tropospheric lifetime. The mass loss fraction is well correlated with the mass fraction of nitrogen-containing compounds, as these species can largely enhance light absorption cross-section and readily undergo photodissociation under UV light.

CHAPTER 1. INTRODUCTION

Biomass-burning organic aerosol (BBOA) emits large amounts of primary organic aerosol as well as volatile organic compounds (VOCs) as products of cellulose pyrolysis (Akagi et al., 2011; De Gouw & Jimenez, 2009; Yokelson et al., 2008). The emitted VOCs can be oxidized in the atmosphere to produce secondary organic aerosol (SOA). Those directly emitted and chemically produced biomass-burning organic aerosol (BBOA) particles further undergo various chemical and physical aging processes, such as condensational growth, evaporation, coagulation, chemical oxidation, hydrolysis, and photolysis, which can change their climate- and health-relevant properties. (Hallquist et al., 2009; Kroll & Seinfeld, 2008; Odum et al., 1996). Recent studies have identified that aerosol and oxidation products of VOC precursors emitted by biomass burning can change the radiative forcing in the range between – 0.8 to +0.6 W/m^2 on the climate system, exerting a large uncertainty on the assessment of historical and future climate change (Myhre et al., 2013; Tsigaridis & Kanakidou, 2018). While many VOCs are emitted in the atmosphere in the event of biomass-burning, furan species have been confirmed as a dominant source of biomass-burning secondary organic aerosol (BBSOA) produced from the hydroxyl (OH) oxidation in the daytime and subsequent gas-phase partitioning (Palm et al., 2020). The primary steps of furan SOA formation have been quantified in a few laboratory and field research studies using mass-spectroscopy (Bierbach et al., 1995; Coggon et al., 2019; Gómez Alvarez et al., 2009; Joo et al., 2019; Liang et al., 2022). The OH oxidation of furan species and formation of SOA from Gómez Alvarez et al., 2009, show the efficiency of SOA formation by obtaining furan

SOA mass concentration of 68.7 $\mu g/m^3$ or less and observed ranges of yield (1.85-8.5%) with carbonyl formation from chemical analysis(Gómez Alvarez et al., 2009). Coggen et al., 2019 evaluated furan species as one of the contributors to ozone and maleic anhydride formation by combining FIREX-AQ measurement with the MCM model study (Coggon et al., 2019). Laboratory results from furan species oxidized by nighttime NO_3 radical show 1.6 - 2.4 % of SOA yield for 5 - 45 $\mu g/m^3$ of generated aerosol mass concentration and require certain conditions, the presence of OH radical production by the ozonolysis, to be a major nighttime sink (Bierbach et al., 1995; Joo et al., 2019).

Along with SOA formation pathways, the change of chemical and physical properties of SOA continues during the atmospheric transport processes including heterogeneous reaction due to photochemical aging. Although multiple oxidations, by gaseous oxidants (such as OH) was traditionally considered the most important pathway of photochemical aging, recent studies highlight that direct UV photolysis can also initiate SOA aging. A few chamber studies have investigated the impact of photolysis on SOA, showing the reduction of SOA mass in the presence of UV light at low OH concentration, in which photolysis could have a substantial contribution to SOA mass loss (Henry & Donahue, 2012; Zawadowicz et al., 2020).

Despite its importance in atmospheric processes, there has been a limited number of studies performed to determine the impact of direct photolysis on SOA. In chamber experiments, it remains challenging to separate direct photolysis from other processes, such as OH oxidation, particle and vapor wall losses, and temperature effect induced by UV light. The typical chamber experiments are conducted on a timescale of less than 1 day, which is shorter than the atmospheric lifetime of SOA. To overcome these

limitations, a few previous studies have utilized the quartz crystal microbalance (QCM) to characterize the mass changes of collected SOA films induced by direct UV photolysis (Baboomian et al., 2020, 2022; Malecha et al., 2018; Malecha & Nizkorodov, 2016). This technique enables long measurements over the timescale relevant to the SOA lifetime (days to 1 week) in a controlled gas environment, which is highly valuable for the photolysis measurements. The QCM technique has been applied in previous studies to measure the volatility, diffusivity, and hygroscopicity of SOA (Liu et al., 2016; Liu et al., 2018a; Liu et al., 2018b). Nevertheless, further understanding of the atmospheric process pathways (i.e. photolysis) of BBSOA is still required to fully understand the impact on the climate. Especially, the implication of direct photolysis on BBSOA has not been studied in the laboratory and key parameters needed to estimate the SOA fate in 3D models are still unknown.

In this study, we produced SOA from the photooxidation of different furan species, including 3-methylfuran, 2-methylfuran, and furfural in an environmental chamber in both dry and humid conditions and measured the chemical composition of the SOA using aerosol mass spectrometry. We grew thin films of SOA materials by collecting the produced SOA particles on crystal sensors. The mass changes of SOA film during direct photolysis under 300 nm and 340 nm UV were continuously monitored using a high-sensitivity, temperature-controlled QCM with dissipation (QCM-D) apparatus. We then correlated chemical characteristics analyzed by a high-resolution time-of-flight aerosol mass spectrometer (HR-ToF-AMS) to investigate typical chemical composition contributing to the photodegradation process. Based on the two-wavelength measurements, we further estimated the photolytically induced mass change of each SOA

type under the solar spectrum and atmospheric implications of photolysis on the BBSOA removal process are discussed.

CHAPTER 2. MATERIALS AND METHODS

2.1 Laboratory chamber experiment: SOA generation

All experiments conducted for SOA formation were performed in the 12 m^3 Georgia Tech Environmental Chamber (GTEC) facility equipped with multiple instruments, which can simultaneously measure aerosol mass concentration and chemical composition of formed SOA, as well as NO, NO_2, O_3, RH, and temperature (Boyd et al., 2015). Wet ammonium sulfate seed particles produced by atomizing 0.015M $(NH_4)_2SO_4$ solution (model 3076, TSI) were injected into the chamber without drying for 20 min. The chamber was operated under two different relative humidity conditions (<5% and ~50% RH), such that the ammonium sulfate particles adopt solid and liquid phase states, respectively. In order to produce SOA, three different types of biomass-burning VOC precursors, 3-methylfuran (98%, Acros Organics), 2-methylfuran (99%, Sigma-Aldrich), and furfural (99%, Sigma-Aldrich) were chosen in this work based on the frameworks used in previous research (Gómez Alvarez et al., 2009; Joo et al., 2019). Nitrous acid (HONO) was used as a source of OH radicals. In this study, HONO was generated by a liquid-phase reaction of 10% sodium nitrite ($NaNO_2$, VWR International) with 10% diluted sulfuric acid (H_2SO_4, VWR International). The mixture of two liquids formed the gas phase HONO which was transferred in a stream of pure air at a flow rate of 5 L/min (Tuet et al., 2017).

After seed particle injection, a VOC precursor was injected into the chamber with HONO. To briefly describe 520-530 ppb of 3-methylfuran, 600-615ppb of 2-methylfuran, 197-201 ppb of furfural, and an excess amount of HONO are added to form

OH radical oxidized SOA in the chamber. After another 1 hr. of mixing, the chamber UV lights (300 nm-400 nm) (Sylvania, 24922) were illuminated to generate OH radical by photolyzing HONO and to initiate the formation of SOA by condensation of oxidized product in each experiment to form SOA. A Scanning Mobility Particle Sizer (SMPS, model 3080, TSI) were used for particle number, volume, and size distribution inside the chamber in the particle size range from 17 nm to 1μm. The concentration of the injected VOC amount was measured using a gas chromatography flame ionization detector (GC-FID, 7890A, Agilent Technologies). The changes of the NO_x cycle from HONO injection were measured by chemiluminescence NO_x monitor for NO (42C, Thermofisher Scientific) and cavity attenuated phase shift (CAPS) for NO_2 concentration. The SOA composition was also monitored by a high-resolution time-of-flight aerosol mass spectrometer (HR-ToF-AMS, Aerodyne Research, Inc.) for aerosol chemical composition (Canagaratna et al., 2007). HR-ToF-AMS is able to identify the fragmentized SOA composition up to the particle size range of 1 μm. HR-ToF-AMS data were analyzed using Igor pro 8.0.4.2 with the standard analysis toolkit of Squirrel v 1.65 and Pika v1.25. Chemical analysis results used in this study are obtained by high-resolution peak fitting and improved ambient method (Canagaratna et al., 2015). In each of the chemical analysis results, chemical characteristics of SOA were obtained over the average 30-minute period at the peak of organic mass concentration of measurement done by HR-ToF-AMS. Details of chemical families retrieved from HR-ToF-AMS data were used for correlation analysis to assess the potential chemical contribution to photolysis. Different chemical compositions were tested in each experiment with modeled mass fraction loss.

2.2 Photolysis of collected SOA film by QCM

To measure the UV photolysis effect of SOA, a quartz-crystal microbalance (QCM, Q-sense explorer, Biolin Scientific AB) was used to measure changes in SOA mass (Liu et al., 2018). For each QCM sensor, water and methanol are used to wash the surface of the sensors. The washed sensors were dried with pure air and then treated with UV-ozone (UV-Ozone cleaner, ProCleaner Plus, Bioforce Nanoscience) for 20 min to clean any contaminants including organics and VOCs on the surface. After the treatment, sensors were placed in QCM for baseline measurements. The baseline is needed to identify the deposited mass on the QCM sensors after SOA collection.

The collection of SOA was conducted using two different methods 1) custom-made single-stage impactor (Liu et al., 2018; Pöschl et al., 2010; Song et al., 2017) and 2) corona discharge unipolar charger (CC-8020, IONER) combined with a nanometer aerosol sampler (TSI 3089) The collection using the custom-made single-stage impactor was connected to the chamber and the chamber air was directly drawn at a flow rate of 4 L/min. The flow rate allotted here gives the cut-off diameter of 100 to 200 nm, which was sufficient to collect the generated SOA in the chamber. The other collection method used a nanometer aerosol sampler with a sensor placed on a negative electrode stage (-10 kV) to collect positively charged particles by a unipolar charger. The flow rate was 1 L/min. By using a unipolar charger, this combined apparatus can largely increase the particle collection efficiency (70-100 %) for particle less than 500 nm compared to our previous studies using a bipolar charger (2-10 %) for PM_1 (Liu et al., 2013, 2016; Liu, Li, et al., 2018a). Both methods can effectively collect SOA mass produced in the chamber with a mode diameter of 300-500 nm in mass-diameter distribution, and we do not anticipate

that different sampling methods significantly affect our results. However, the second method can produce more uniform particle deposition thus preferred for the QCM analysis.

The SOA-laden QCM sensor was placed in a window module flow cell (Biolin Scientific, Q-sense QWM-401) and the SOA mass was analyzed under different UV light wavelengths (300 nm, 340 nm, and dark) (UV LED M300L4 and 340L4, Thorlabs) using QCM as shown in Appendix Figure A1. The sampling frequency of QCM is roughly 1 s. Since particle sizes collected on the sensors were sufficient to form a thin film, the samples were analyzed directly without any further treatment The height of the LED light was affixed to be identical throughout the entire experiment to maintain the UV light intensities. The UV photon flux was measured by a power energy meter (PM100D with S405C sensor, Thorlabs). The QCM chamber was purged with a zero-air flow (737-15, Adeco) at a flow rate of 0.03 L/min. The zero air was split into two flow lines to be used for dry and humid air downstream of the flow. The flow of this experiment was adjusted to only dry flow at the RH below 1 %. The lights were alternatively turned on and turned off every 10 min for a clear distinction between photolysis and non-photolysis period. The light-off periods between light-on periods represented evaporation without active direct photolysis, which can be used to determine the volatility of the photolysis products. Dark experiments without turning on the UV light were also conducted to measure the evaporative mass loss of SOA without photolysis. The data were reported as the mass fraction remaining of SOA, defined as SOA mass during the dark or photolytic aging experiment normalized by the initial SOA mass deposited on the QCM sensor. The analysis of the SOA mass fraction remaining has excluded the mass of ammonium sulfate

seed particles for each experiment, determined based on the HR-ToF-AMS analysis measured for chamber aerosol during the sampling period.

2.3 Modeling of SOA mass loss by photolysis under solar spectrum

To demonstrate the potential impact of photolysis on SOA in atmospheric conditions, a numerical model was performed as described in section Appendix A1. This model specifically focused on describing the effect of atmospheric photolysis on furan SOA.

Since not all SOA mass deposited on the sensor undergoes photolysis, we expressed relevant variables obtained from experimentally measured photolytic decay under each lamp using exponential functions. The exponential function can be displayed as following equations 1 and 2. In these equations, we considered the non-photolabile fraction (A0 for 300 nm and B0 for 340 nm), the photolabile fraction (A1 for 300 nm and B1 for 340 nm), and the photolysis rate (k1 for 300 nm and g1 for 340 nm). The study assumed that the sum of the unreactive fraction and the photolabile fraction of SOA is equal to 1. The parameters for these photolysis rate constants for each experiment were calculated with respect to the organic fraction measured by HR-ToF-AMS and absorbance measured by UV-Vis spectrometer (DT-Mini and USB4000, Ocean Optics). Furthermore, the mass absorption efficiency (MAE) for each compound was determined based on the absorbance measurements as described in Appendix section A2.

$$m_{Lamp,300\,nm} = A_0 + A_1 \exp(-k_1 t) \quad \text{(Equation 1)}$$

$$m_{Lamp,340\,nm} = B_0 + B_1 \exp(-g_1 t) \quad \text{(Equation 2)}$$

In order to investigate the mass decay of furan SOA through photolysis under solar spectrum conditions, we employed a scaling factor derived from the standard solar irradiance spectrum (ASTM G-173-03, National Renewable Energy Laboratory) as shown in equation 3. Where F_L is the photon flux, σ_λ is the absorption cross-section, and $\Phi_{L,\lambda}$, quantum yields of lamps are assumed to be constant within the wavelength range of each lamp.

$$scaling\ factor = \frac{\int F(\lambda)_{solar}\,\sigma_\lambda d\lambda}{\int F(\lambda)_{Lamp}\,\sigma_\lambda d\lambda} = \frac{J_{solar}}{J_{lamp}} \qquad \text{(Equation 3)}$$

$$J = \int F(\lambda) \cdot \phi(\lambda) \cdot \sigma(\lambda) \cdot d\lambda \qquad \text{(Equation 4)}$$

The fractions between J_{lamp} and J_{solar} were used to derive the scaling factors of each lamp. With the application of scaling factors, the mass fraction loss of each experiment was regenerated equivalent to solar radiation. With the wavelength-dependent absorption cross-section, the photolysis rate constant of solar radiation (J_{solar}) was also calculated (equation 4). This approach allowed us to accurately assess the impact of solar radiation on the degradation of furan SOA, providing valuable insights into its environmental fate and potential implication.

CHAPTER 3. RESULTS AND DISCUSSION

3.1 Mass loss observation of Furan SOA under various conditions

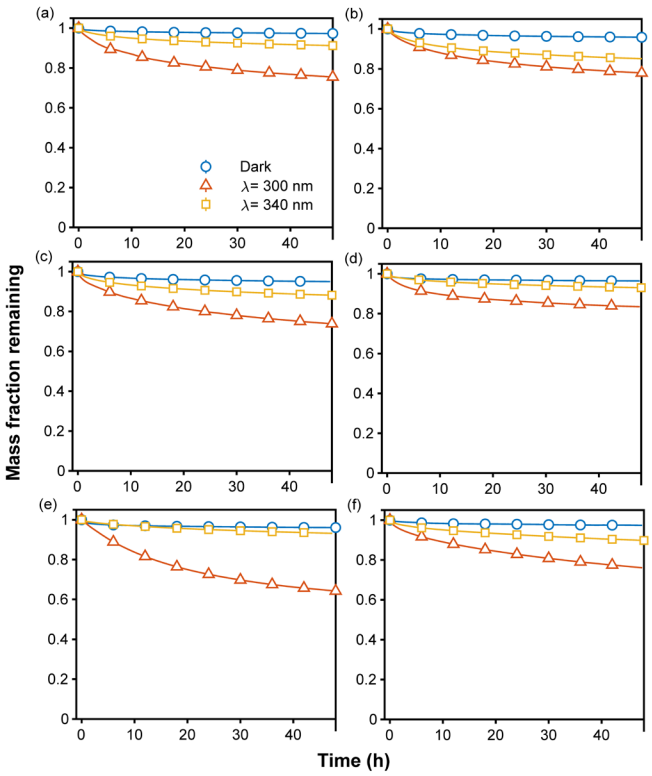

Figure 1. Time series profile of SOA mass fraction remaining measured by QCM for photolysis under 300 nm (red), 340 nm (yellow) UV light irradiation, and during dark (blue) condition (a) 3-methylfuran SOA generated under dry chamber condition, (b) 3-methylfuran SOA generated under humid chamber condition, (c) 2-methylfuran SOA generated under dry chamber condition, (d) 2-methylfuran SOA generated under humid chamber condition, (e) furfural SOA generated under dry condition, and (f) furfural SOA generated under humid chamber condition

A series of experiments confirm that SOA produced from different furan precursors can undergo significant photolytic mass loss for both 300 nm and 340 nm UV irradiation. Figure 1 shows the measured time profiles of mass fraction remaining for SOA generated from 3 different VOC precursors under different chamber RH. The

aerosol formation for each precursor, chamber RH, SOA mass loading on the QCM sensor, and density of organics observed for all chamber experiments are listed in Table A1. A large aerosol formation discovered at higher RH for 3-methylfuran and 2-methylfuran could be led by water uptake. ΔM_0 is calculated based on the density of organics were calculated based on the H:C and O:C ratio presented by Kuwata et al., 2012 (Kuwata et al., 2012). The final percentage of SOA mass loss after 48 hr. photolysis under dark, 300 nm and 340 nm UV light in the QCM of each experiment is summarized in Table A2. The mass fraction loss observed under dark conditions (blue line with circular marker) is measured to be close to or less than 5% in all measured data. This mass loss is due to the evaporation of semi-volatile organic carbon (SVOCs) that occurred in the QCM chamber condition, which is determined by the intrinsic volatility and possibly diffusivity of SOA material (Liu et al., 2016). The mass fraction losses for photolytic aging experiments under 300 nm and 340 nm UV irradiation are higher than the dark baseline over the entire 48 hr. experiment, indicating significant photolytic mass losses. For SOA produced at dry conditions, the percentage of mass loss after hr. photolysis under 300 nm UV was the greatest for furfural SOA (35.8 %), followed by 2-methylfuran SOA (26.2%), and 3-methylfuran SOA (24.5%), hence the least mass fraction remains on the sensor. Meanwhile, SOA produced in a humid chamber showed less mass fraction loss compared to dry SOA, furfural, 2-methylfuran, and 3-methylfuran SOA at 23.9 %, 16.5 %, and 22.0 %, respectively. Such data from mass fraction loss in the dry and humid conditions confirms that all obtained BBSOA formed under dry conditions gets lost by photolysis under 300 nm light. Compared with photolytic aging experiments under 300 nm UV, the mass loss fractions induced by 48 hr. photolysis

under 340 nm UV were less, because of weaker light absorption and possibly lower quantum yield at the longer wavelength, although the 340 nm UV light used in the study had a stronger light intensity than the 300 nm light as shown in Figure A2.

Considering the results obtained from the experiments, the mass loss of furan SOA by photolysis shows the dependence on light energy emitted. We anticipate that the wavelength of the light affected the amount of energy absorbed by the SOA, which could potentially contribute to the quantum yield of the SOA. As the SOA is more susceptible to light energy, the number of molecules undergoing photolysis can be larger to induce SOA mass loss. A comparison of the experiments with each light condition confirms that the mass fraction loss of BBSOA could be directly affected by the light wavelength. Especially, the result shows a much higher mass loss of SOA during the photolysis of 300 nm light than 340 nm light. While the distribution of mass loss varied under 340 nm light, the changes of mass during the light illumination are much greater than in the dark condition, which confirms that the BBSOA under 340 nm light illumination is still susceptible to absorbing light energy to undergo photolysis.

Although photolysis in various wavelengths of light photolyzes a substantial portion of the organic aerosol mass, the RH effect during the formation of SOA is also highlighted. The water uptake during the formation of SOA can change the hygroscopicity of the SOA which could affect refractive index of the aerosol and phase state of SOA during the photolysis (Tao et al., 2014). Wong et al., 2015 and Baboomian et al., 2019 measured an increase in mass loss rate by a factor of 2-3 during photolysis on α-pinene SOA at elevated RH from laboratory chamber and QCM experiments

(Baboomian et al., 2020; Wong et al., 2015). However, it is worth noting that BBSOA formed under dry conditions produces much higher mass loss than the BBOA formed in humid conditions in this study. The deviation between water contribution to SOA formation and photolysis impact is more significant under 300 nm light, indicating that RH condition during the formation of SOA can play a crucial role in the mass loss rate due to the water uptake. Although the photolysis experiments are maintained at less than 1% of RH condition, we expect that the RH condition during the photolysis cannot be negligible in the mass loss rate by aerosol liquid water content. We conclude that the absolute mass fraction losses are a combination of the evaporation, formation of semi-volatile organic compound (SVOC), and photo-dissociation of SOA, and the dominant impact by photolysis was driven to the overall mass loss measured by the QCM. Mang et al., 2008 reported that the study for limonene-derived SOA on the filter and in aqueous solutions, in which the formation of CO, CH_4, acetone, and other VOCs was observed during the photolysis via Norrish Type I and II reactions (Mang et al., 2008). Thus, any potential formation of secondly generated aerosols during photolysis still requires further research.

3.2 Relationship between chemical characteristics of Furan SOA and mass fraction loss

The photolysis behavior of SOA can be affected by several factors. The actinic flux of UV irradiation and light absorption cross-section of SOA combined can determine the photon flux absorbed by the SOA, which can in turn determine the upper limit of the photolysis rate (equation 4). The chemical composition, such as functional groups, can determine both light absorption and the quantum yield, thus influencing the photolysis

rates and photo-labile fraction. The mass loss rate and mass and mass remaining fraction can be also influenced by the volatility of photolysis products, as photolysis may produce SVOCs that slowly evaporate even without UV light. Using SOA chemical composition data measured by the HR-ToF-AMS, we explored potential relationships between the mass loss fraction and the mass fraction of different chemical families. The fraction parameterization results from HR-ToF-AMS are described for each type of experiment in Figure A3 and the results of the parameterized values are applied in Figure 2. Due to the light-absorbing properties of the organic nitrate, we include the CHN, $CH_{(y)}ON$, $CHO_{(y)}N$, and NO families as nitrogen-containing compounds of this parameterization analysis (Farmer et al., 2010; Laskin et al., 2015). Figure 2(a) shows the relationship between the net mass loss fraction obtained under 300 nm after 48 hr. UV light irradiation and the nitrogen-containing compound fraction that is positively associated with a slope of $2.3x + 0.032$ and r^2 of 0.55, which shows the highest correlation among all compositions. This indicates that nitrogen-containing species can play an important role in photolysis. The chemical compositions in the generated furan SOA are expected to be related to the photolysis to have different mass decay rates observed in the QCM experiment. One plausible explanation is that the nitrogen-containing compounds are likely to be the brown carbon aerosol present in chromophores which absorbs light and is likely to be lost by photobleaching (Adler et al., 2019; Laskin et al., 2015; O'Brien & Kroll, 2019). These results can be compared with previous studies on the photolytic mass loss of different types of SOA measured online in chamber studies and offline by the QCM and other techniques. For example, chamber studies by O'Brien and Kroll (2019) suggest that α-pinene SOA under 300-400 nm UV light undergoes rapid initial mass

decay followed by a much slower mass loss rate, and 70%-90% SOA is photo-recalcitrant with negligible photolytic degradation (O'Brien & Kroll, 2019). Our study confirms that a large fraction of SOA derived from furan species can be non-photolabile.

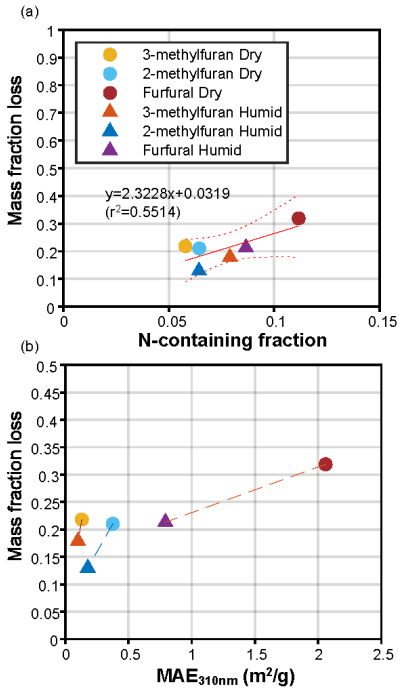

Figure 2. Chemical characteristics verses the mass fraction loss at 300 nm UV irradiation (a) N-containing fraction and (b) with mass absorption efficiency (MAE) at 310 nm measured by UV-visible spectrometer

Here, we use MAE at 310 nm which represents the similar light energy applied in the experiment due to the uncertainties of methanol soluble extracts in the wavelength below 305 nm on the UV-Vis spectrometer (Figure 2(b)). The pattern of MAE_{310nm} of furan SOA shows that higher MAE 310 nm values are observed from the SOA generated in dry conditions. A higher MAE_{310nm} is associated with a higher mass fraction loss for 300 nm UV photolysis. Detailed analysis on the light absorption of furan SOA produced under different chamber RH and possible chemical mechanisms of brown carbon formation are discussed elsewhere (Joo et al., 2023). Overall, this agreement indicates

that furfural SOA has higher light absorbing properties, such as wavelength-dependent aerosol optical property than others, in which the mass loss is associated with the enhancement of the MAE 310 nm by the formation condition of SOA resulting in a higher mass fraction loss by the photolysis. The difference in light absorption properties between SOA of the same precursor produced under dry and humid chamber conditions can well explain the difference in the photolabile fraction under 300 nm UV.

We note that the slope between mass fraction loss and the nitrogen-containing fraction is higher than unity, indicating that photolysis of nitrogen-containing species alone does not fully explain the photo-labile fraction of SOA. In addition, the role of RH in the process of formation of SOA involved in the formation of carbonyl, such as glyoxal, methylglyoxal as described in the previous study, which will eventually form hemiacetal product (aldehyde or ketone) (Nguyen et al., 2011). Previous research, Wong et al., 2015 utilized the analysis method adopted by Ng et al., 2011 to describe the trend of the functional group identified by HR-ToF-AMS and identified a substantial decrease of f43 (carbonyl) fraction during the photolysis period from α-pinene SOA (Ng et al., 2011; Wong et al., 2015). Interestingly, the relationship with CHO^+ fragment detected at m/z 29 containing carbonyl functional group in this study did not show a significant relationship with the mass fraction loss, as well as from the $C_2H_3O^+$, m/z 43 which could be contributed by carbonyl, alcohols, and ethers. Although the CHO fraction is considered as carbonyl functional group, the study results do not identify the direct relationship with RH effect on carbonyl formation as well as the carbonyl functional group to mass fraction loss. Therefore, our result from this study is not consistent with the photolysis experiment data of α-pinene SOA in a chamber. The disagreement on the

functional group is likely due to the major chemical oxidation pathways of ozonolysis and photooxidation. However, due to the contribution of nitrogen-containing compounds generated during the formation of SOA, it is possible that other chemical functional groups, such as amines, amides, imines, etc., could play a crucial role in photolytic mass loss mechanisms.

3.3 Atmospheric implication

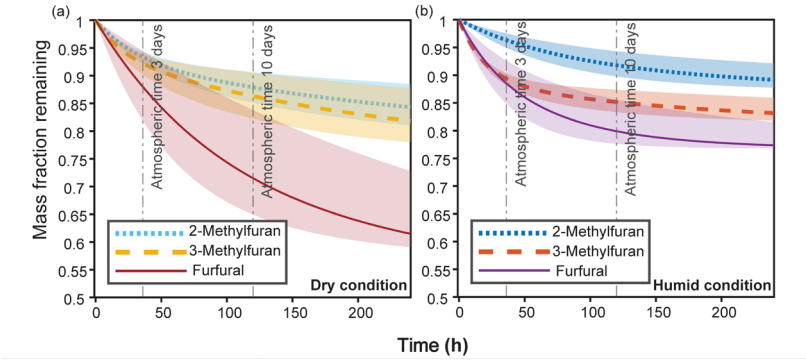

Figure 3. Photolytic mass loss curve under solar spectrum radiation for each SOA type (a) photolytic mass decay with SOA formed under dry condition and (b) photolytic mass decay with SOA formed under humid condition. Dashed line refers to the potential mass loss of furan-derived BBOA in the boundary layer and lower free troposphere.

The photolysis curves under the solar spectrum radiation are generated for each SOA type in Figure 3 and the potential mass loss after 240 hr. of photolysis is listed in Table A3. In order to identify the potential mass loss of furan-derived SOA by photolysis, we further estimate decays with an exponential fit and categorized the photolabile (A0 for 300 nm and B0 for 340 nm), non-photolabile fraction (A1 for 300 nm and B1 for 340 nm), and photolysis rate (k1 for 300 nm and g1 for 340 nm) for mid-range as shown in Table 1. The values of photolabile, non-photolabile fractions, and mass decay rate determined by exponential fitting based on the experiments are applied and used bi-exponential fitting to obtain the mass loss under the solar spectrum as described in materials and method section 2.3. We project photolysis in atmospheric conditions, where model calculations predict less mass loss compared to the experimental results when compared with the same photolysis time. There are two reasons for this effect, (1) the wider solar spectrum incorporated for photolysis impact is less affected by the mass

decrease, (2) the intensity of light directly involved in the photon energy absorbed on SOA, which would strongly decrease the mass fraction measured by QCM. Therefore, we anticipate less mass loss under the solar spectrum by applying a scaling factor between the solar spectrum and lights. The model estimates of potential mass fraction loss in the solar spectrum showed the highest loss in a mass fraction on furfural SOA, which agrees with the experimental results. The dashed vertical lines remark the potential decay in mass fraction of furan-derived BBOA in the boundary layer and lower free troposphere, indicating that the mass fraction of SOA derived from 3-methylfuran, 2-methylfuran, and furfural can be decreased significantly with photolysis under the solar spectrum. Clearly, there are uncertainties shown as shaded areas in this model. The contribution to these uncertainties is determined by the under-represented scales between the two lights and the solar spectrum which is not constrained in this model. Therefore, the mid-range mass loss and its rate reported in this study are likely to underestimate or overestimate the primary photolytic mass loss. However, the photolysis effect of such SOA may be the important fate of SOA in the atmospheric condition.

Table 1. Photolabile, non-photolabile, and photolysis rate for each SOA type

		A0	A1	k1 (hr^{-1})	B0	B1	g1 (hr^{-1})
Dry	**3-methylfuran**	0.76	0.24	0.057	0.94	0.061	0.074
	2-methylfuran	0.77	0.23	0.058	0.93	0.071	0.064
	Furfural	0.62	0.38	0.043	0.27	0.73	0.00088
Humid	**3-methylfuran**	0.81	0.19	0.068	0.89	0.11	0.082
	2-methylfuran	0.87	0.13	0.087	0.95	0.049	0.026
	Furfural	0.77	0.23	0.049	0.92	0.083	0.046

CHAPTER 4. CONCLUSION

To assess the importance of photolysis in the atmosphere, the mass fraction loss with respect to the solar irradiation spectrum was estimated. Using the experimentally determined photolabile, non-photolabile, and photolysis rate, the mass fraction loss under the solar spectrum is to be between 10-40 % over 10 days of continuous photolysis. Given that the average lifetime of SOA in the atmosphere is approximately 1-2 weeks, this result provides a very broad estimation indicating that the photolysis can be an important sink of BBSOA in the atmosphere. Also, we hypothesized that the dependence of photolysis on the chemical characteristics of SOA is due to the nitrogen-containing fraction. Especially, higher N-containing fraction exhibited the higher mass fraction loss, which likely contain amine, amides, and imines. These functional groups can be lost by photodegradation and chemical loss during photolysis. This finding suggests that the photolysis reaction on biomass burning precursor-derived SOA could potentially cause a decrease in mass concentration in the atmospheric condition. The photolytic decomposition pathways of the SOA and the analysis of the production of SOA during the photolysis still require further research in detail. However, this study shows ranges of impact on SOA mass from different biomass-burning VOC precursors under specific UV wavelengths, as well as in the solar spectrum. Therefore, the study results have a significant implication for the projection of climate change by improving the representation of organic aerosol in the atmospheric model by providing knowledge related to biomass burning events.

APPENDIX A. SUPPORTING INFORMATION

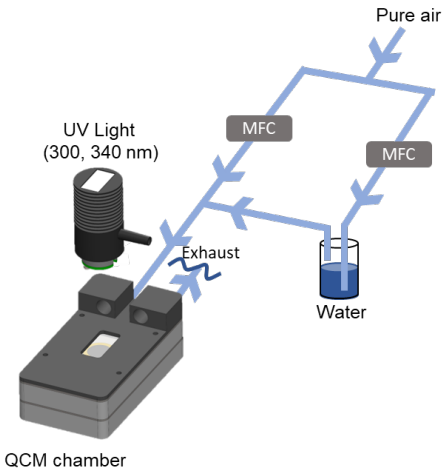

Figure A1. Experimental setup using quartz crystal microbalance (QCM)

A.1 Modeling of SOA mass loss by photolysis under solar spectrum

In this part of the study, the developed model included the standard solar spectrum coupled to the flux of lights to simulate the potential impact of photolysis on SOA. The initial relationship between lamp frequency offsets (Hz) to total irradiance (W/m^2) was obtained by light calibration. We assume that the photon flux of the lamp $f_{Lamp,\lambda}$ is based on the known shape of light intensity. To demonstrate the potential impact of photolysis on SOA in atmospheric conditions, the conversion of lamp frequency offset to total irradiance is applied based on the light calibration as shown in Figure 2. The calculated total irradiance and solar irradiance spectrum (ASTM G-173-03, National Renewable Energy Laboratory) are converted into photon flux using Planck-Einstein relation, h is Plank's constant ($6.626 \times 10^{-34}\,(J/s)$), c is a speed of light ($3.00 \times 10^{8}(m/s)$), λ is

a wavelength (nm), e is photon energy ($J/photon$), E is irradiance spectrum ($W/m^2 \cdot nm$), and F is photon flux ($Photons/cm^2 \cdot s^2 \cdot nm$) using equation 1 and 2.

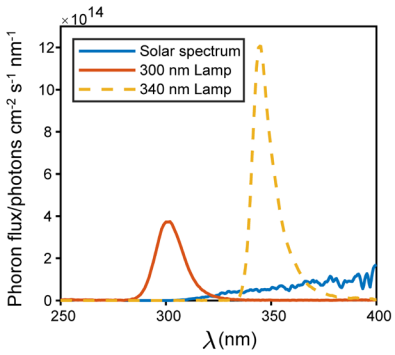

Figure A2. Spectral photon flux density of 300 nm light, 340 nm light, and solar spectrum (ASTM G-173-03)

$$e_\lambda = h\frac{c}{\lambda} \quad \text{(Equation 1)}$$

$$F_\lambda = \frac{E_\lambda}{e_\lambda} \quad \text{(Equation 2)}$$

Based on the power output of the lamp by the manufacturers' specification, the lamp photon flux distribution ($F_{Lamp,\lambda}$) is derived by applying the correction factor of C_{Lamp} (Equation 3). Solar irradiance spectrum is also converted to photon flux based on e_λ, where e_λ is the photon energy associated with a wave of light with a frequency and $E_{solar,\lambda}$ is solar irradiance spectrum (W/m^2 nm) (Equation 4).

$$C_{Lamp} = \frac{E_1}{\int f_{Lamp,\lambda} e_\lambda d\lambda};\ F_{Lamp,\lambda} = C_{Lamp} f_{Lamp,\lambda} \quad \text{(Equation 3)}$$

$$F_{solar,\lambda} = \frac{E_{solar,\lambda}}{e_\lambda} \quad \text{(Equation 4)}$$

With the wavelength-dependent absorption cross-section, the photolysis rate constant of solar radiation (j_{solar}) is also calculated based on Equation 5. The fractions between j_{lamp} and j_{solar} are used to derive the scaling factors of each lamp. With the application of scaling factors, the mass fraction loss of each experiment is regenerated equivalent to solar radiation. The scaling factors of photolysis rates between lamps and the solar radiation could be calculated using the following equation 6-8:

$$J = \int F_\lambda \Phi_\lambda \sigma_\lambda F d\lambda \quad \text{(Equation 5)}$$

$$J_{L1} = \int F_{L1,\lambda} \sigma_\lambda \Phi_{L1,\lambda}\, d\lambda = \Phi_{L1} \int F_{L1,\lambda} \sigma_\lambda\, d\lambda \quad \text{(Equation 6)}$$

$$J_{L2} = \int F_{L2,\lambda} \sigma_\lambda \Phi_{L2,\lambda}\, d\lambda = \Phi_{L2} \int F_{L2,\lambda} \sigma_\lambda\, d\lambda \quad \text{(Equation 7)}$$

$$J_{solar<\lambda_{cut}} = \int_{280\ nm}^{\lambda_{cut}} F_{solar,\lambda} \sigma_\lambda \Phi_{solar,\lambda}\, d\lambda \quad \text{(Equation 8)}$$

$$= \Phi_{solar<\lambda_{cut}} \int_{280\ nm}^{\lambda_{cut}} F_{solar,\lambda} \sigma_\lambda\, d\lambda$$

Where F_L is the photon flux of the lamp, σ_λ is the absorption cross-section, and $\Phi_{L,\lambda}$, quantum yields of lamps are assumed to be constant within the wavelength range of each lamp. The absorbance at a specific wavelength is calculated using the following equation 9:

$$\sigma_\lambda = \log(10) \frac{Abs_\lambda}{NL} = \log(10) \frac{Abs_\lambda}{\rho L} MW_{SOA} \quad \text{(Equation 9)}$$

Abs_λ is the absorbance measured by UV-Vis as a function of wavelength from the previous study (Joo et al., 2023). N is the molecule concentration of SOA in the extract, ρ

is the mass concentration of the extraction solution, and L is the optical depth (2.5 m) used during UV-vis spectrometry measurement (DT-Mini and USB4000, Ocean Optics). In this study, the choice of molecular weight of the SOA was assumed to be 200 g/mol.

The derivation of the scaling factor from lamps to two ranges of the solar spectrum can be done as R_L (Equation 10-11).

$$R_{L1} = \frac{J_{solar<\lambda_{cut}}}{J_{L1}} = \frac{\int F_{L1,\lambda}\sigma_\lambda \, d\lambda}{\int_{280\ nm}^{\lambda_{cut}} F_{solar,\lambda}\sigma_\lambda \, d\lambda} \quad \text{(Equation 10)}$$

$$R_{L2} = \frac{J_{solar>\lambda_{cut}}}{J_{L2}} = \frac{\int F_{L2,\lambda}\sigma_\lambda \, d\lambda}{\int_{\lambda_{cut}}^{400\ nm} F_{solar,\lambda}\sigma_\lambda \, d\lambda} \quad \text{(Equation 11)}$$

The method calculating the decay rates of the photolysis of furan-derived SOA is done by following equation 12-15.

$$m_{L1} = A_0 + A_1 \exp(-k_1 t) \quad \text{(Equation 12)}$$

$$m_{L2} = B_0 + B_1 \exp(-g_1 t) \quad \text{(Equation 13)}$$

If, $A_0 < B_0$ (Equation 14)

$$f_1 = A_0; f_2 = (B_0 - A_0)\exp(-k_1 R_{L1} t)\,; f_3 = (1 - B_0)\exp(-R_{L1}k_1 t - R_{L2}g_1 t)$$

If, $B_0 < A_0$ (Equation 15)

$$f_1 = B_0; f_2 = (A_0 - B_0)\exp(-g_1 R_{L2} t)\,; f_3$$
$$= (1 - A_0)\exp(-R_{L1} k_1 t - R_{L2} g_1 t)$$

To fit the experimental data, we use an exponential model, A_0 and B_0 represent the fraction of the un-photolyzable SOA, A_1 and B_1 as photolyzable fraction of SOA with decay rate of k_1 and g_1 respectively for each lamp. The summation of the components $A_0 + A_1$ and $B_0 + B_1$ are normalized to 1 and the photolysis curve under the solar radiation is generated by equation 16.

$$m_{solar} = f_1 + f_2 + f_3 \qquad \text{(Equation 16)}$$

Table A2. Experimental condition measured by GC-FID, HR-ToF-AMS, SMPS, and QCM

Experiment	**3-methylfuran**		**2-methylfuran**		**Furfural**	
RH condition	**Dry (<5%)**	**Humid (50-55%)**	**Dry (<5%)**	**Humid (50-55%)**	**Dry (<5%)**	**Humid (50-55%)**
ΔHC **(ppb)**	520.67 ± 1.94	533.58 ± 2.65	614.63 ± 1.87	603.44 ±4.90	197.49 ±3.45	201.64 ± 3.28
ΔM_0 **(μg/m³)**	164.00± 0.48	287.62± 1.37	109.63 ± 0.70	163.64± 1.27	195.23 ± 0.40	193.48 ± 1.44
Elemental ratio (H:C, O:C)	1.56, 1.24	1.54, 1.20	1.39, 1.49	1.41, 1.55	1.15, 1.38	1.20, 0.94
Density of organic (g/cm³)	1.68	1.66	1.85	1.87	1.9	1.67
Mass on QCM sensor (μg)	17.19, 9.39, 10	4.31, 1.55, 5.33	5.92, 5.23, 9.43	11.65, 13.7, 4.90	9.31, 8.79, 14.76	4.04, 5.52, 4.92

Table A3. Final organic mass fraction loss under different over 48 hr. light illumination

	SOA precursor	Dark	300 nm	340 nm
Dry	3-methylfuran	2.71%	24.52%	8.88%
	2-methylfuran	5.14%	26.17%	11.85%
	Furfural	3.91%	35.80%	6.79%
Humid	3-methylfuran	4.16%	22.04%	14.88%
	2-methylfuran	3.57%	16.52%	6.98%
	Furfural	2.58%	23.91%	10.19%

A.2 Prediction of mass absorption efficiency (MAE)

The mass absorption efficiency at 310 nm is estimated based on the measured absorbance (abs_λ) followed by equation 17 for each compound from the UV-vis spectrometer described previously. In this part of the study, organic aerosol samples are collected on 47 mm Teflon filters (2 μm pore size, Pall Corporation) during the peak aerosol mass concentration. Collected organic aerosols are dissolved in methanol and water to extract soluble organic aerosol. However, in this specific study, we only use the absorbance of organic aerosol dissolved in a methanol solution to obtain any soluble organic aerosols deposited on the filter samples. Detailed descriptions of filter collection were described in Joo et al., 2023 (Joo et al., 2023).

$$MAE_{310\,nm}\left(m^2/g\right) = \frac{\frac{\sum_{305\,nm}^{315nm} abs_\lambda}{11}}{Total\ soluable\ organic\ aerosol\ (\ g\ \ m^{-2})} \qquad \text{(Equation 17)}$$

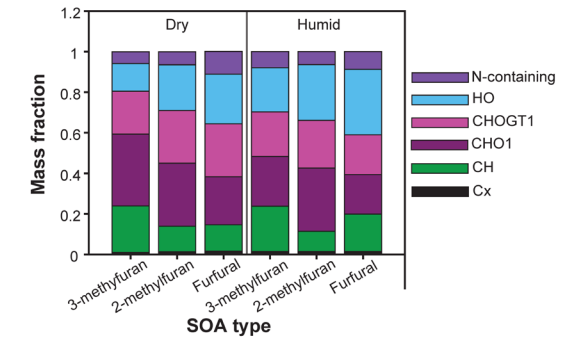

Figure A3. Typical composition fraction of furan SOA derived from laboratory chamber experiment

Table A4. Summary of relative reduction (%) of BBOA due to photolysis under solar spectrum by hours

	SOA precursor	24 hr.	48 hr.	72 hr.	240 hr.	3-day ambient (36 hr.)	10-day ambient (120 hr.)
Dry	3-methylfuran	6.1%	9.1%	11.0%	18.2%	7.8%	13.7%
	2-methylfuran	5.0%	7.9%	9.8%	15.7%	6.7%	12.1%
	Furfural	8.5%	15.2%	20.6%	38.5%	12.0%	28.5%
Humid	3-methylfuran	8.7%	11.8%	13.3%	16.8%	10.6%	14.8%
	2-methylfuran	2.5%	4.6%	6.2%	10.8%	3.6%	8.2%
	Furfural	8.6%	13.6%	16.7%	22.6%	11.4%	20.1%

REFERENCES

Adler, G., Wagner, N. L., Lamb, K. D., Manfred, K. M., Schwarz, J. P., Franchin, A., Middlebrook, A. M., Washenfelder, R. A., Womack, C. C., Yokelson, R. J., & Murphy, D. M. (2019). Evidence in biomass burning smoke for a light-absorbing aerosol with properties intermediate between brown and black carbon. *Aerosol Science and Technology*, *53*(9), 976–989. https://doi.org/10.1080/02786826.2019.1617832

Akagi, S. K., Yokelson, R. J., Wiedinmyer, C., Alvarado, M. J., Reid, J. S., Karl, T., Crounse, J. D., & Wennberg, P. O. (2011). Emission factors for open and domestic biomass burning for use in atmospheric models. *Atmospheric Chemistry and Physics*, *11*(9). https://doi.org/10.5194/acp-11-4039-2011

Baboomian, V. J., Crescenzo, G. V., Huang, Y., Mahrt, F., Shiraiwa, M., Bertram, A. K., & Nizkorodov, S. A. (2022). Sunlight can convert atmospheric aerosols into a glassy solid state and modify their environmental impacts. *Proceedings of the National Academy of Sciences of the United States of America*, *119*(43). https://doi.org/10.1073/pnas.2208121119

Baboomian, V. J., Gu, Y., & Nizkorodov, S. A. (2020). Photodegradation of Secondary Organic Aerosols by Long-Term Exposure to Solar Actinic Radiation. *ACS Earth and Space Chemistry*, *4*(7), 1078–1089. https://doi.org/10.1021/acsearthspacechem.0c00088

Bierbach, A., Barnes, I., & Becker, K. H. (1995). Product and kinetic study of the oh-initiated gas-phase oxidation of Furan, 2-methylfuran and furanaldehydes at ≈ 300 K. *Atmospheric Environment*, *29*(19), 2651–2660. https://doi.org/10.1016/1352-2310(95)00096-H

Boyd, C. M., Sanchez, J., Xu, L., Eugene, A. J., Nah, T., Tuet, W. Y., Guzman, M. I., & Ng, N. L. (2015). Secondary Organic Aerosol (SOA) from Nitrate Radical Oxidation of Monoterpenes: Effects of Temperature, Dilution, and Humidity on Aerosol Formation, Mixing, and Evaporation. *Atmospheric Chemistry and Physics*, *15*(13), 7497–7522. https://doi.org/10.5194/acp-15-7497-2015

Canagaratna, M. R., Jayne, J. T., Jimenez, J. L., Allan, J. D., Alfarra, M. R., Zhang, Q., Onasch, T. B., Drewnick, F., Coe, H., Middlebrook, A., Delia, A., Williams, L. R., Trimborn, A. M., Northway, M. J., DeCarlo, P. F., Kolb, C. E., Davidovits, P., & Worsnop, D. R. (2007). Chemical and microphysical characterization of ambient aerosols with the aerodyne aerosol mass spectrometer. *Mass Spectrometry Reviews*, *26*(2), 185–222. https://doi.org/10.1002/mas.20115

Canagaratna, M. R., Jimenez, J. L., Kroll, J. H., Chen, Q., Kessler, S. H., Massoli, P., Hildebrandt Ruiz, L., Fortner, E., Williams, L. R., Wilson, K. R., Surratt, J. D., Donahue, N. M., Jayne, J. T., & Worsnop, D. R. (2015). Elemental ratio measurements of organic compounds using aerosol mass spectrometry: characterization, improved calibration, and implications. *Atmospheric Chemistry and Physics*, *15*(1), 253–272. https://doi.org/10.5194/acp-15-253-2015

Coggon, M. M., Lim, C. Y., Koss, A. R., Sekimoto, K., Yuan, B., Gilman, J. B., Hagan, D. H., Selimovic, V., Zarzana, K. J., Brown, S. S., Roberts, J. M., Müller, M., Yokelson, R., Wisthaler, A., Krechmer, J. E., Jimenez, J. L., Cappa, C., Kroll, J. H., de Gouw, J., & Warneke, C. (2019). OH chemistry of non-methane organic gases (NMOGs) emitted from laboratory and ambient biomass burning smoke: evaluating the influence of furans and oxygenated aromatics on ozone and secondary NMOG formation. *Atmospheric Chemistry and Physics*, *19*(23), 14875–14899. https://doi.org/10.5194/acp-19-14875-2019

De Gouw, J., & Jimenez, J. L. (2009). Organic Aerosols in the Earth's Atmosphere. *Environmental Science & Technology*, *43*(20), 7614–7618. https://doi.org/10.1021/es9006004

Farmer, D. K., Matsunaga, A., Docherty, K. S., Surratt, J. D., Seinfeld, J. H., Ziemann, P. J., & Jimenez, J. L. (2010). Response of an aerosol mass spectrometer to organonitrates and organosulfates and implications for atmospheric chemistry. *Proceedings of the National Academy of Sciences of the United States of America*, *107*(15). https://doi.org/10.1073/pnas.0912340107

Gómez Alvarez, E., Borrás, E., Viidanoja, J., & Hjorth, J. (2009). Unsaturated dicarbonyl products from the OH-initiated photo-oxidation of furan, 2-methylfuran and 3-methylfuran. *Atmospheric Environment*, *43*(9), 1603–1612. https://doi.org/10.1016/j.atmosenv.2008.12.019

Hallquist, M., Wenger, J. C., Baltensperger, U., Rudich, Y., Simpson, D., Claeys, M., Dommen, J., Donahue, N. M., George, C., Goldstein, A. H., Hamilton, J. F.,

Herrmann, H., Hoffmann, T., Iinuma, Y., Jang, M., Jenkin, M. E., Jimenez, J. L., Kiendler-Scharr, A., Maenhaut, W., … Wildt, J. (2009). The formation, properties and impact of secondary organic aerosol: current and emerging issues. *Atmospheric Chemistry and Physics*, *9*(14), 5155–5236. https://doi.org/10.5194/acp-9-5155-2009

Henry, K. M., & Donahue, N. M. (2012). Photochemical Aging of α-Pinene Secondary Organic Aerosol: Effects of OH Radical Sources and Photolysis. *The Journal of Physical Chemistry A*, *116*(24), 5932–5940. https://doi.org/10.1021/jp210288s

Joo, T., Rivera-Rios, J. C., Takeuchi, M., Alvarado, M. J., & Ng, N. L. (2019). Secondary Organic Aerosol Formation from Reaction of 3-Methylfuran with Nitrate Radicals. *ACS Earth and Space Chemistry*, *3*(6), 922–934. https://doi.org/10.1021/acsearthspacechem.9b00068

Joo, T., Machesky, J. E., Zeng., L., Hass-Mitchell, T., Weber, R. J., Gentner, D. R., Ng, N. L. (2023), Secondary Brown Carbon Formation from Photooxidation of Furans from Biomass Burning. submitted

Kroll, J. H., & Seinfeld, J. H. (2008). Chemistry of secondary organic aerosol: Formation and evolution of low-volatility organics in the atmosphere. *Atmospheric Environment*, *42*(16), 3593–3624. https://doi.org/10.1016/j.atmosenv.2008.01.003

Kuwata, M., Zorn, S. R., & Martin, S. T. (2012). Using Elemental Ratios to Predict the Density of Organic Material Composed of Carbon, Hydrogen, and Oxygen. *Environmental Science & Technology*, *46*(2), 787–794. https://doi.org/10.1021/es202525q

Laskin, A., Laskin, J., & Nizkorodov, S. A. (2015). Chemistry of Atmospheric Brown Carbon. In *Chemical Reviews* (Vol. 115, Issue 10). https://doi.org/10.1021/cr5006167

Liang, Y., Weber, R. J., Misztal, P. K., Jen, C. N., & Goldstein, A. H. (2022). Aging of Volatile Organic Compounds in October 2017 Northern California Wildfire Plumes. *Environmental Science & Technology*, *56*(3), 1557–1567. https://doi.org/10.1021/acs.est.1c05684

Liu, P., Li, Y. J., Wang, Y., Bateman, A. P., Zhang, Y., Gong, Z., Bertram, A. K., & Martin, S. T. (2018a). Highly Viscous States Affect the Browning of Atmospheric Organic Particulate Matter. *ACS Central Science*, *4*(2), 207–215. https://doi.org/10.1021/acscentsci.7b00452

Liu, P., Li, Y. J., Wang, Y., Gilles, M. K., Zaveri, R. A., Bertram, A. K., & Martin, S. T. (2016). Lability of secondary organic particulate matter. *Proceedings of the National Academy of Sciences*, *113*(45), 12643–12648. https://doi.org/10.1073/pnas.1603138113

Liu, P., Song, M., Zhao, T., Gunthe, S. S., Ham, S., He, Y., Qin, Y. M., Gong, Z., Amorim, J. C., Bertram, A. K., & Martin, S. T. (2018b). Resolving the mechanisms of hygroscopic growth and cloud condensation nuclei activity for organic particulate matter. *Nature Communications*, *9*(1), 4076. https://doi.org/10.1038/s41467-018-06622-2

Liu, P., Zhang, Y., & Martin, S. T. (2013). Complex refractive indices of thin films of secondary organic materials by spectroscopic ellipsometry from 220 to 1200 nm. *Environmental Science and Technology*, *47*(23). https://doi.org/10.1021/es403411e

Malecha, K. T., Cai, Z., & Nizkorodov, S. A. (2018). Photodegradation of Secondary Organic Aerosol Material Quantified with a Quartz Crystal Microbalance. *Environmental Science & Technology Letters*, *5*(6), 366–371. https://doi.org/10.1021/acs.estlett.8b00231

Malecha, K. T., & Nizkorodov, S. A. (2016). Photodegradation of Secondary Organic Aerosol Particles as a Source of Small, Oxygenated Volatile Organic Compounds. *Environmental Science & Technology*, *50*(18), 9990–9997. https://doi.org/10.1021/acs.est.6b02313

Mang, S. A., Henricksen, D. K., Bateman, A. E., Andersen, M. P. S., Blake, D. R., & Nizkorodov, S. A. (2008). Contribution of carbonyl photochemistry to aging of atmospheric secondary organic aerosol. *Journal of Physical Chemistry A*, *112*(36). https://doi.org/10.1021/jp804376c

Myhre, G., Shindell, D., Bréon, F., Collins, W., Fuglestvedt, J., Huang, J., Koch, D., Lamarque, J., Lee, D., Mendoza, B., Nakajima, T., Robock, A., Stephens, G., Takemura, T., & Zhang, H. (2013). Anthropogenic and natural radiative forcing . In T. Q. D. P. G. T. M. A. S. B. J. N. A. X. Y. B. V. M. P. Stocker (Ed.), *Climate change 2013: The physical science basis. Contribution of working group I to the fifth assessment report of the Intergovernmental Panel on Climate Change* (pp. 659–740). Cambridge University Press .

Ng, N. L., Canagaratna, M. R., Jimenez, J. L., Chhabra, P. S., Seinfeld, J. H., & Worsnop, D. R. (2011). Changes in organic aerosol composition with aging inferred from aerosol mass spectra. *Atmospheric Chemistry and Physics*, *11*(13), 6465–6474. https://doi.org/10.5194/acp-11-6465-2011

Nguyen, T. B., Roach, P. J., Laskin, J., Laskin, A., & Nizkorodov, S. A. (2011). Effect of humidity on the composition of isoprene photooxidation secondary organic aerosol. *Atmospheric Chemistry and Physics*, *11*(14), 6931–6944. https://doi.org/10.5194/acp-11-6931-2011

O'Brien, R. E., & Kroll, J. H. (2019). Photolytic Aging of Secondary Organic Aerosol: Evidence for a Substantial Photo-Recalcitrant Fraction. *Journal of Physical Chemistry Letters*, *10*(14). https://doi.org/10.1021/acs.jpclett.9b01417

Odum, J., Hoffmann, T., Bowman, F., Collins, D., Flagan, R., & Seinfeld, J. (1996). Gas/Particle Partitioning and Secondary Organic Aerosol Yields. *Environmental Science & Technology*, *30*(8), 2580–2585.

Palm, B. B., Peng, Q., Fredrickson, C. D., Lee, B. H., Garofalo, L. A., Pothier, M. A., Kreidenweis, S. M., Farmer, D. K., Pokhrel, R. P., Shen, Y., Murphy, S. M., Permar, W., Hu, L., Campos, T. L., Hall, S. R., Ullmann, K., Zhang, X., Flocke, F., Fischer, E. V., & Thornton, J. A. (2020). Quantification of organic aerosol and brown carbon evolution in fresh wildfire plumes. *Proceedings of the National Academy of Sciences*, *117*(47), 29469–29477. https://doi.org/10.1073/pnas.2012218117

Pöschl, U., Martin, S. T., Sinha, B., Chen, Q., Gunthe, S. S., Huffman, J. A., Borrmann, S., Farmer, D. K., Garland, R. M., Helas, G., Jimenez, J. L., King, S. M., Manzi, A., Mikhailov, E., Pauliquevis, T., Petters, M. D., Prenni, A. J., Roldin, P., Rose, D., … Andreae, M. O. (2010). Rainforest Aerosols as Biogenic Nuclei of Clouds and Precipitation in the Amazon. *Science*, *329*(5998), 1513–1516. https://doi.org/10.1126/science.1191056

Song, M., Liu, P., Martin, S. T., & Bertram, A. K. (2017). Liquid–liquid phase separation in particles containing secondary organic material free of inorganic salts. *Atmospheric Chemistry and Physics*, *17*(18), 11261–11271. https://doi.org/10.5194/acp-17-11261-2017

Tao, J. C., Zhao, C. S., Ma, N., & Liu, P. F. (2014). The impact of aerosol hygroscopic growth on the single-scattering albedo and its application on the NO2 photolysis rate coefficient. *Atmospheric Chemistry and Physics*, *14*(22). https://doi.org/10.5194/acp-14-12055-2014

Tsigaridis, K., & Kanakidou, M. (2018). The Present and Future of Secondary Organic Aerosol Direct Forcing on Climate. *Current Climate Change Reports*, *4*(2), 84–98. https://doi.org/10.1007/s40641-018-0092-3

Tuet, W. Y., Chen, Y., Xu, L., Fok, S., Gao, D., Weber, R. J., & Ng, N. L. (2017). Chemical oxidative potential of secondary organic aerosol (SOA) generated from the photooxidation of biogenic and anthropogenic volatile organic compounds. *Atmospheric Chemistry and Physics*, *17*(2). https://doi.org/10.5194/acp-17-839-2017

Wong, J. P. S., Zhou, S., & Abbatt, J. P. D. (2015). Changes in secondary organic aerosol composition and mass due to photolysis: Relative humidity dependence. *Journal of Physical Chemistry A*, *119*(19). https://doi.org/10.1021/jp506898c

Yokelson, R. J., Christian, T. J., Karl, T. G., & Guenther, A. (2008). The tropical forest and fire emissions experiment: laboratory fire measurements and synthesis of campaign data. *Atmospheric Chemistry and Physics*, *8*(13), 3509–3527. https://doi.org/10.5194/acp-8-3509-2008

Zawadowicz, M. A., Lee, B. H., Shrivastava, M., Zelenyuk, A., Zaveri, R. A., Flynn, C., Thornton, J. A., & Shilling, J. E. (2020). Photolysis Controls Atmospheric Budgets of Biogenic Secondary Organic Aerosol. *Environmental Science & Technology*, *54*(7), 3861–3870. https://doi.org/10.1021/acs.est.9b07051